Journal of Power Sources 196 (2011) 2530–2538

Contents lists available at ScienceDirect

Journal of Power Sources

journal homepage: www.elsevier.com/locate/jpowsour

XPS investigations of the proton exchange membrane fuel cell active layers aging: Characterization of the mitigating role of an anodic CO contamination on cathode degradation

Valérie Parry[a,*], Grégory Berthomé[a], Jean-Charles Joud[a], Olivier Lemaire[b], Alejandro A. Franco[b]

[a] Grenoble Institute of Technologies – SIMaP, 1130 rue de la Piscine, 38402 Saint-Martin d'Hères, France
[b] Atomic and Alternative Energies Commission of France – CEA/DRT/LITEN/DETH – Laboratory of Components for Fuel Cells and Electrolyzers, and of Modeling (LCPEM), 17, Rue des Martyrs, 38054 Grenoble cedex 9, France

ARTICLE INFO

Article history:
Received 30 June 2010
Received in revised form 8 October 2010
Accepted 7 November 2010
Available online 13 November 2010

Keywords:
PEMFC
XPS
Active layers aging
CO contamination
Carbon corrosion

ABSTRACT

This paper presents new results from XPS quantitative characterizations of cathode catalyst layers aged in a PEMFC with an anode operated under pure hydrogen and air and with 5 ppm CO contaminated hydrogen. Both oxygen rich and oxygen poor zones of the cathode catalyst layer were analyzed in order to show up heterogeneous degradation linked with gas distribution. The detailed chemical XPS analysis of the aged samples demonstrates in particular that in our operating conditions, the catalyst layer aging is mainly attributed to the oxidation of the carbon catalyst-support. A loss of the Nafion® ionomer in the cathode is also highlighted by XPS. Furthermore, the characterization of the cathodic catalyst layer chemical composition when CO is introduced in the anode side shows that the catalyst layer degradation is lower. These results are in agreement with the experimental-modeling work by Franco et al. [1] demonstrating that anodic CO contamination decreases the reverse proton pumping effect between the cathode and the anode and enhances the PEMFC durability.

1. Introduction

Large-scale deployment of proton exchange membrane fuel cells (PEMFCs) is facing today two major challenges: decrease of the cost and increase of the lifetime [2–4]. The most important performance degradation phenomena have been identified, such as water management, membrane degradation, carbon corrosion, Pt-based catalyst dissolution/migration/recrystallisation, contaminants impact, etc. [5–13].

In this context, we have proposed multiscale mechanistic models to describe cathode damage, in particular carbon corrosion process [14–17]. Carbon corrosion process is especially enhanced under current-cycled operating conditions, where an anodic ORR, pumping protons from the cathode to the anode, is induced by O_2 permeation from the cathode to the anode.

Several experimental studies have also indicated that the cathodic carbon catalyst-support corrosion is exacerbated by the presence of O_2 in the anode [18]. The cathode carbon catalyst-support oxidation [15–19] and CO_2 formation proceed as:

$$R\text{–}C_{surf}\text{–}H + 2H_2O \rightarrow R\text{–}H + CO_{2(g)} + 4H^+ + 4e^- \quad (1)$$

wherein C_{surf} denotes surface carbon species [20]. Although carbon corrosion increases with increasing potential, surface oxides groups are prone to form at potentials lower than 0.9 V [21].

This carbon corrosion can induce significant cathode microstructural changes and thus a degradation of the PEMFC performance; a dramatic catalyst active surface area loss can be also induced by this cathode carbon corrosion phenomenon [7,22]. It is believed that misdistribution or local interruptions in the anode hydrogen supply improve O_2 permeation from the cathode into the anode [23]. The formation of liquid water drops in the anodic channel could also locally block the hydrogen access to the electrode [24]. In-line direct gas mass spectroscopy analysis has successfully detected intermittent CO_2 emission peaks in exhausted gas from the cathode, indicating that carbon corrosion especially occurs during the load cycle in the PEMFC [23,25,26].

The presence of CO in the anode feed stream can have a major impact on PEMFC performances through the poisonning of the anodic catalyst. However, under current-cycled operating conditions, it has been demonstrated that the anodic CO contamination can be used to mitigate the cathode carbon catalyst-support corrosion phenomena which will lead to an increase of the MEA

Abbreviations: CCM, catalyst coated membrane; CL, catalyst layer; EW, equivalent weight; GDL, gas diffusion layer; MEA, membrane electrodes assembly; HOR, hydrogen oxidation reaction; ORR, oxygen reduction reaction; PEMFC, proton exchange membrane fuel cell; PTFE, polytetrafluoroethylene; XPS, X-ray photoelectron spectroscopy.

* Corresponding author. Tel.: +33 476826671; fax: +33 476826667.
E-mail address: valerie.parry@simap.grenoble-inp.fr (V. Parry).

0378-7753/$ – see front matter © 2010 Elsevier B.V. All rights reserved.
doi:10.1016/j.jpowsour.2010.11.027

durability. This is explained by the anodic reactivity between the CO and the membrane crossover O_2, the last one being the "driving force" of the reverse proton current between the electrodes [1].

Experimental in situ and ex situ analytical techniques are useful to characterize the evolution of the PEMFC performance as well as the physical and chemical structure of their components: electrochemical characterizations (polarization curves, cyclic voltammetry, electrochemical impedance spectrometry, etc.), gas and water analyses, transmission and scanning electron microscopies, differential electrochemical mass spectrometry, local measurements (current densities, temperatures, etc.) associated to specific experiments (half-cells, rotating ring-disc electrode, infrared spectroscopy, etc.). Among these techniques, X-ray photoelectron spectroscopy (XPS) is a quantitative and surface-sensitive tool widely used for the determination of chemical composition and chemical state of materials [27–31]. Recently it has been used to study chemical changes of the catalyst layer [32–34] and polymer membrane [35–37] induced by degradation during PEMFC operation. However, further investigations still remain necessary to precise more deeply how materials degrade.

In the first part of this paper, we present new results from XPS quantitative characterizations of cathode catalyst layer (CL) aged in a PEMFC with an anode operated under pure hydrogen and with a cathode operated under air. The second part is dedicated to the analysis of the aged cathode CL when CO is introduced in hydrogen. Both oxygen rich and oxygen poor zones were analyzed in order to show up heterogeneous MEA degradation linked with an unsuitable gas distribution. The concentration changes of the CL elements including C, F, Pt, O and S, were analyzed in detail before and after several hundred hours of operation in a fuel cell, and the chemical changes of CL components were identified.

2. Experimental

2.1. Fuel cell experiments

Experiments were performed with CCM-type home-made 25 cm^2 MEA based on a Nafion® NRE212CS membrane (50 μm thickness) from DuPont. Anode and cathode catalyst layers (Nafion® EW 1100 from Dupont and commercial Pt/C ETEK with 20 wt% platinum with Carbon Vulcan XC72), as well as carbon felt gas diffusion layers (H2315-T10A from Freudenberg), have been deposited on the membrane. The platinum catalyst loadings were 0.19 ± 0.01 mg cm^{-2} and 0.24 ± 0.01 mg cm^{-2} on the anode and cathode sides, respectively. The ionomer/carbon weight ratios were 2.84 for both anode and cathode. A microporous layer (Carbon Vulcan XC72 (0.7 mg cm^{-2}) with PTFE (0.21 mg cm^{-2})) was deposited on the gas diffusion layers. The MEAs were hot pressed under 3.5 MPa, at 130 °C, for 3.5 min. Gas tightness was ensured using silicone gaskets from Silfox.

All cells were operated at 70, with H_2 and air at 1.6×10^5 Pa, and 60% relative humidity for both anode and cathode sides. As shown in Fig. 1, anode and cathode gases were fed under counter-flow mode. After a 16 h conditioning phase under 0.8 A cm^{-2} constant current, a current cycle was applied. The first 22 h were performed under pure hydrogen and air, before introducing 5 ppm of CO in hydrogen for the experiments with pollutant. The current cycle consists of two successive 30 min phases with current densities set to 0.108 A cm^{-2} and 0.540 A cm^{-2}. Flow rates follow current according to a stoechiometry of 1.2 in the anode and 2 in the cathode. During the current increase and current decrease phases the flux rates follow the current with a delay shorter than 1 s, with a current increase time (1 min) longer than the current decrease time. These experiments aim to be model experiments facilitating the transient oxygen crossover from the cathode to the anode and thus exacerbating MEA degradation.

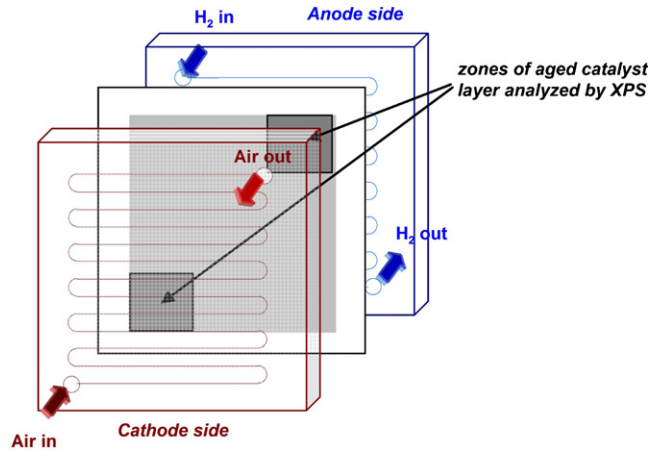

Fig. 1. Scheme of the anode and cathode gas feeding into the single fuel cell (counter-flow mode) showing the areas of aged catalyst layers analyzed by XPS.

2.2. XPS analysis

The XPS analyses were carried out in a Vacuum Generator XR3E2 apparatus with a Mg Kα X-ray source at 15 kV, 20 mA operating condition. Analyses were carried out at an angle of 90° between the sample surface and the hemispherical analyzer. Pressure in the sample chamber was less than 10^{-8} Pa. Sample dimensions were 1 cm × 1 cm and the analyzed average area is about 40 mm^2. The fresh sample was taken from an unused MEA. The aged samples were taken from both the oxygen rich (inlet) and oxygen poor (outlet) zone of the cathode CL and from both the hydrogen rich and hydrogen poor zone of the anode CL (Fig. 1). Four CLs were analyzed: fresh, after 350 h and 550 h operation under pure H_2, after 630 h with 5 ppm CO-contaminated H_2. Only the cathode side results are presented in this study.

Survey spectra, from 0 to 1100 eV binding energy, were collected with a data rate of 2 points per eV, and signal-averaged over three scans. The high-resolution spectra were collected with a data rate of 10 points per eV and signal-averaged over 40 scans for Pt4f and 20 scans for the other photoelectron lines. The pass energy was set at 30 eV for both survey and high-resolution spectra resulting in an energy resolution of approximately 0.1 eV. The electron binding energy scale was calibrated by setting the C1s peak of graphitized carbon at 284.6 eV. Spectra were analyzed using a freeware software package, Fitt 1.2 (GTK) (Photoelectron Spectroscopy Lab, Seoul National University) with Shirley background corrections.

An estimation of the elemental composition (atomic %) of the samples was obtained from the intensities of the photoelectron lines, using a standard quantitative XPS analysis. The atomic concentrations were derived from the areas of the characteristic photoelectron lines after substraction of a Shirley background, divided by the sensitivity factor.

One of the biggest drawbacks in surface analysis with XPS is the reproductibility in absolute quantification, in the order of 10 at.%. The approach taken mainly depends on the subsequent data processing methods applied: background substraction, choice of sensitivity factors, peak area measurments, deconvolution and curve fitting. Thus, being able to obtain an accurate relative quantitative analysis requires that all photoelectron lines be fitted in exactly the same way. Binding energy values are choosen from data available in the literature [38]. The Gaussian/Lorentzian peak shape mixing ratio was determined by the fit of the Au4f peak from a clean gold sample. The binding energy values were first adjusted to fit the slope of the photoelectron line for the fresh sample, then they were fixed in the range of ±0.1 eV for the aged samples. Hence one can expect, for the major photoelectron lines, a relative accuracy of 1%

Table 1
Elemental quantification of the cathode catalyst layers analyzed by XPS. A relative accuracy of 1% for C, F and O is expected.

Element	Surface composition in at.%					
	Fresh	After 350 h	After 550 h		After 630 h (CO)	
		Inlet	Inlet	Outlet	Inlet	Outlet
C	53.7	53.1	57.2	56.5	56.1	56.0
F	40.5	34.5	28.1	34.5	31.3	31.7
O	4.5	11.0	13.7	7.6	11.6	10.9
Pt	0.5	0.3	0.2	0.5	0.2	0.3
S	0.8	1.1	0.8	0.9	0.8	1.1

on the calculated concentrations.

2.3. Sample preparation for XPS analysis

The GDL and the top of the CL were peeled off with specific adhesive tape. This proceeding was repeated until the complete removal of the microporous layer. For preparation of the first sample, the attendance of catalyst particules was checked by scanning electron microscopy. Then the surface was gently cleaned with a brush and dry nitrogen flow. The preparation process was the same for the whole of the samples. No subsequent contamination arising from the adhesive tape was observed on the survey spectra.

3. Results and discussion

3.1. XPS analysis of the fresh catalyst layer

Survey spectrum of the fresh sample is reported in Fig. 2(a). The atomic concentrations derived from the areas of the characteristic photoelectron lines are reported in Table 1. The sample composition is dominated by fluorine and carbon and additionally small extents of sulfur, platinum and oxygen are mesurable.

The fitted high resolution spectra for carbon, oxygen, fluorine and platinum of the fresh cathode CL are displayed in Figs. 3(a), 4(a), 5(a) and 6(a). The spectrum of the sulfur S2p is not presented because the low ionization cross-section of this photoelectron line does not allow a detailed qualitative analysis of the spectrum. The measured binding energies and the related chemical bonding of each component are reported in Table 2.

The C1s XPS spectrum, displayed in Fig. 3(a), is fitted by two dominant peaks at the binding energies of 284.5 eV and 291.7 eV. The first is assigned to C–C bonds and is related to the carbon catalyst-support composed of graphitized carbon. The second peak is related to the C–F bonds in the Nafion® ionomer used as binder. A smaller component at higher binding energy (293.1 eV) is assigned to $C–F_3$ and/or $C–OF_2$ groups [39]. Two additional minor carbon-containing components between these two peaks are related to the oxidized forms of carbon (C–O type bonds at 286.4 eV and C=O type bonds at 288.9 eV).

Fluorine is associated to the Nafion® ionomer. The F1s spectrum in Fig. 5(a) can be fitted by two peaks at 688.9 eV and 691.6 eV. The first corresponds to $C–F_2$ bonds in the Nafion® PTFE backbone. The second peak is related to the $C–F_3$ end-group or $C–OF_2$ groups in the polymer pendant side-chain.

The sulfur and the oxygen signals are related to the sulfuric acid functional groups and oxygen atoms in the perfluoro-ether groups of the Nafion®. Thus oxygen in Nafion® is in two different binding states. For each sulfuric acid group, three oxygen atoms are bonded to a sulfur atom and two oxygen atoms in the side-chain polymer are in an ether configuration. From this, the expected ratios of these two oxygen species and of the oxygen and the sulfur concentrations are about 3:2 and 5:1 respectively.

The O1s photoelectron line of the fresh sample, displayed in Fig. 5(a), is split off into two peaks corresponding to the two different binding states of oxygen in Nafion® as described above. The low binding energy peak at 532.3 eV is related to oxygen atoms in the ether configuration whereas the peak around 535 eV is linked to oxygen atoms in the sulfuric acid group. The large difference of binding energies (about 3 eV) allows us to clearly separate the two components.

In order to check the validity of our XPS decomposition, CL component surface concentrations derived from XPS and weight ratios are presented in Table 3 together with theoretical concentrations expected for Nafion® EW1100. The Nafion® used as binder consists of approximately 30.8 at.% carbon, 60.0 at.% fluorine, 7.7 at.% oxygen and 1.5 at.% sulfur [40,41]. Considering a confidence interval of 1% for our XPS decomposition, the ionomer elements concentrations determined by XPS are in good agreement with the expected data.

The Pt4f spectrum describing the platinum chemical state in the fresh CL sample is displayed in Fig. 6(a). The photoelectron line splits off into two states which arise from the spin orbit coupling of the 4f sub shell. The relative intensity of the two peaks which reflect the degeneracies of the final states 4f5/2 and 4f7/2 is fixed to 3/4. The distance between the two peaks is fixed to 3.3 eV according to pure Pt value [38]. Two oxidation states are observed. The low binding energy value of 71.4 eV for the 4f7/2 peak is assigned to metallic

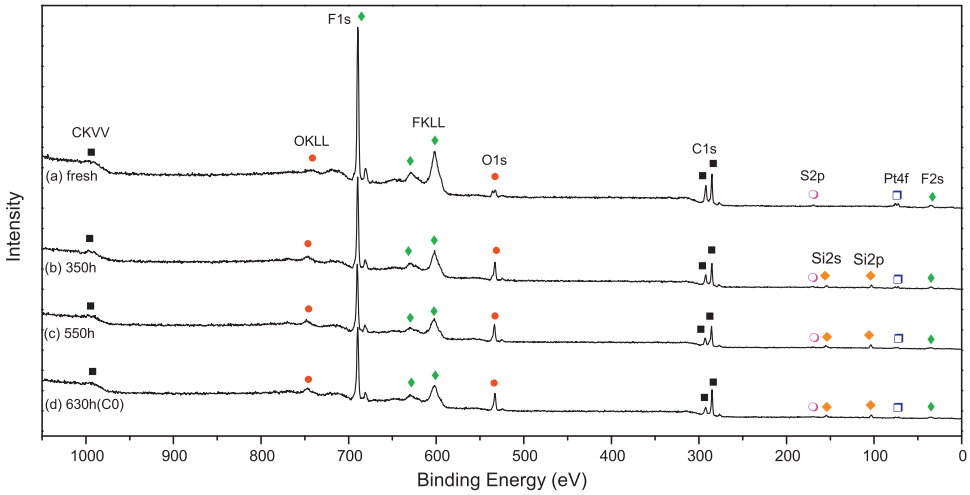

Fig. 2. Survey spectra from (a) the fresh cathode catalyst layer, the inlet zone of the cathode catalyst layers aged for (b) 350 h (c) 550 h under pure H_2 and air (d) 630 h under H_2 with 5 ppm CO and air.

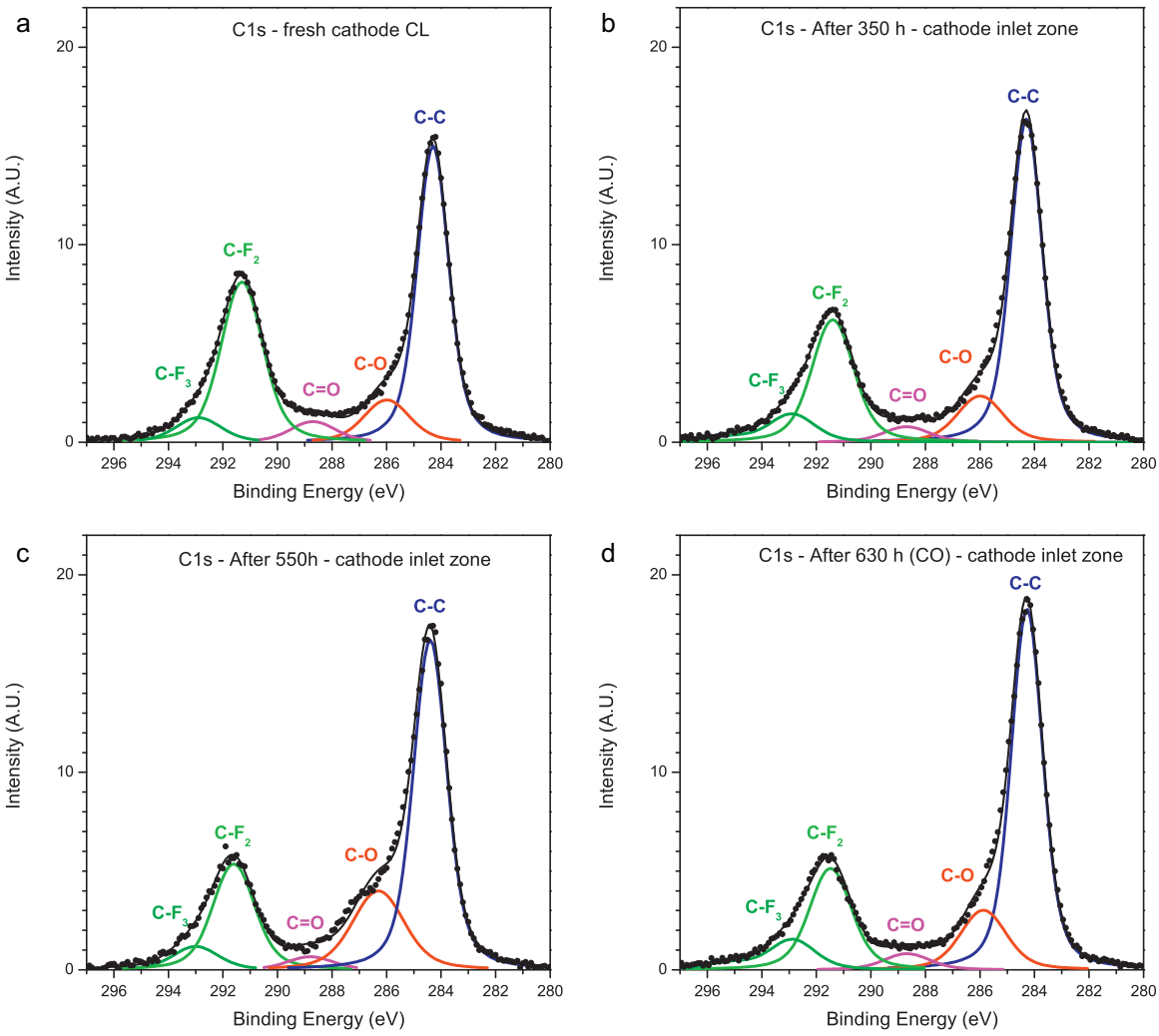

Fig. 3. C1s spectra from (a) the fresh cathode CL, the inlet zone of the cathode catalyst layers aged for (b) 350 h (c) 550 h under pure H_2 and air (d) 630 h under H_2 with 5 ppm CO and air.

platinum, while the highest one at 72.7 eV is assigned to oxidized platinum. The ratio between these two states of platinum is 4.2. The platinum/catalyst-support weight ratio presented in Table 3 is close to the expected value of 20 wt% of platinum. The separation process of the microporous layer from the cathode CL is indeed effective. The surface of the cathode CL does not contain some carbon from the microporous layer otherwise the carbon content would have been seemingly increased.

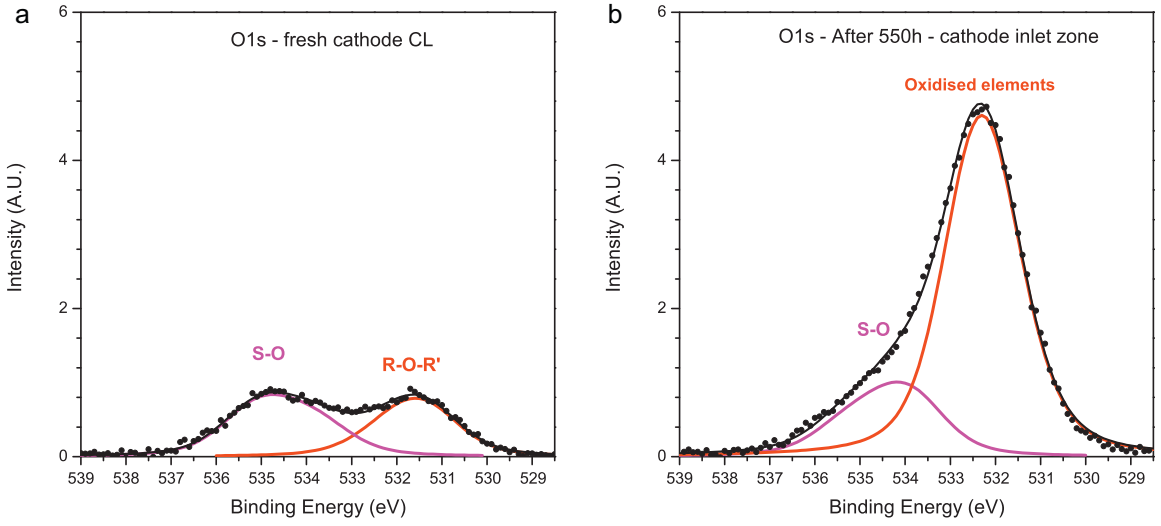

Fig. 4. O1s spectra from (a) the fresh cathode CL (b) the inlet zone of the cathode catalyst layer aged for 550 h under pure H_2 and air.

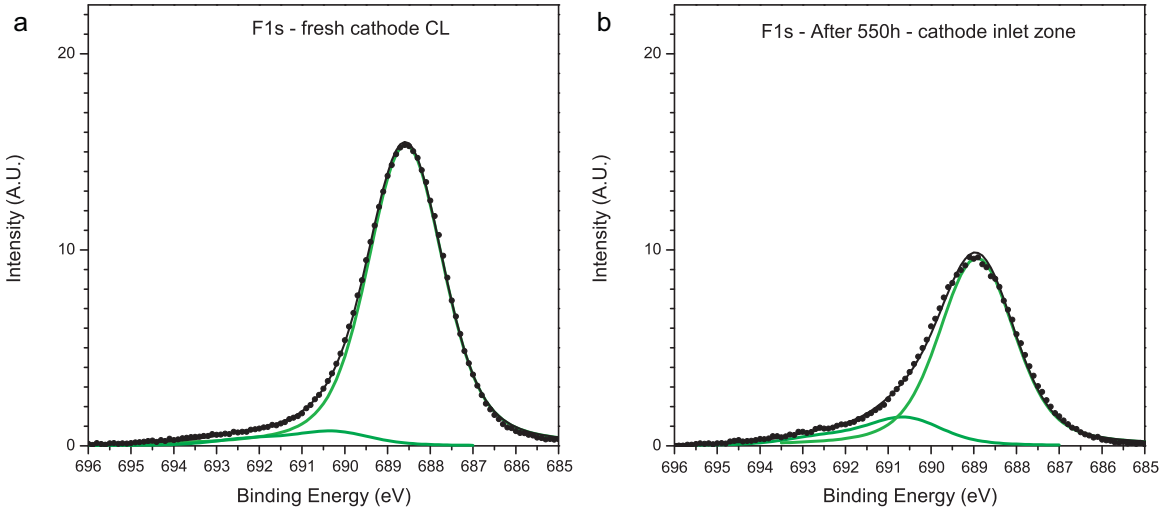

Fig. 5. F1s spectra from (a) the fresh cathode CL (b) the inlet zone of the cathode catalyst layer aged for 550 h under pure H_2 and air.

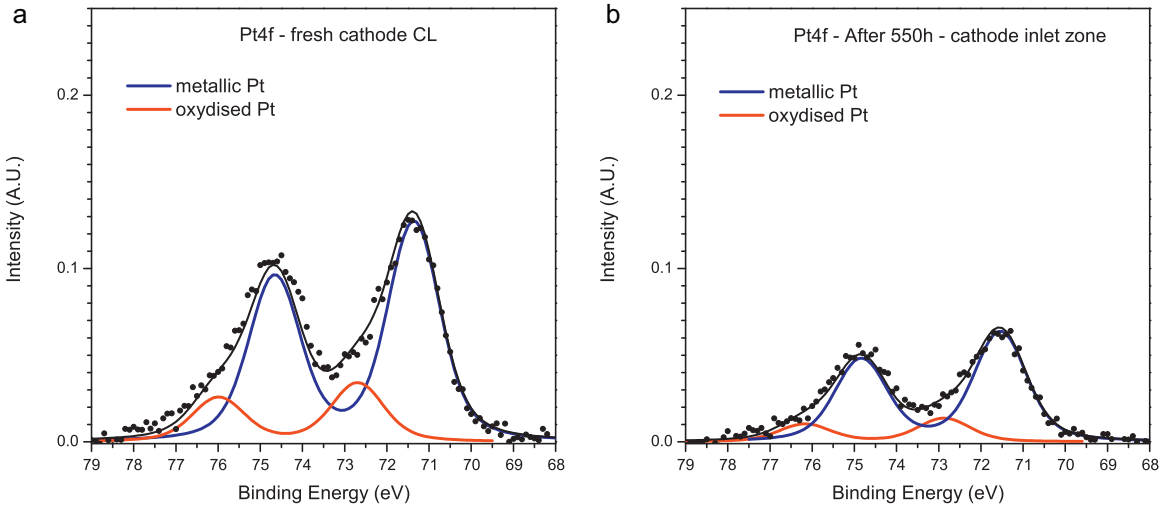

Fig. 6. Pt4f spectra from (a) the fresh cathode CL (b) the inlet zone of the cathode catalyst layer aged for 550 h under pure H_2 and air.

3.2. PEMFC aging under pure H_2

3.2.1. Performance degradation

Fig. 7(a) shows the cell voltage evolutions with time under pure hydrogen for two durations. The performance decrease is linear: 0.13 mV h^{-1} for 0.108 A cm^{-2}, and 0.48 mV h^{-1} for 0.54 A cm^{-2}. A detailed discussion about these performance results can be found in [1]. As explained above, we will focus here on the XPS analyses performed on the MEA at different aging stages.

Table 2
Measured binding energies and related chemical bondings of each components of the cathode catalyst layers analyzed by XPS. A relative accuracy of 1% for C, F and O is expected.

Element	Component	Chemical bonding	Binding energy (eV) (±0.1 eV)	Surface composition (at.%)					
				Fresh	After 350 h Inlet	After 550 h Inlet	Outlet	After 630 h (CO) Inlet	Outlet
Pt	Catalyst	Pt–Pt	71.4	0.39	0.25	0.19	0.43	0.18	0.28
Pt	Catalyst	Pt–O	72.7	0.11	0.06	0.04	0.06	0.06	0.07
C	C-support	C–C	284.5	25.2	27.8	30.0	32.8	30.9	29.6
C	C-support	C–O	286.4	5.1	5.7	10.9	7.4	7.3	7.1
C	C-support	C=O	288.9	2.5	1.9	1.6	0.6	2.0	3.8
C	Nafion®	C–F_2	291.7	17.9	13.8	11.9	12.5	11.4	14.2
C	Nafion®	C–OF_2, C–F_3	293.1	3.0	4.0	2.9	2.7	4.5	1.9
O	Oxidized elm. and Nafion®	C–O, C=O	532.3	2.0	8.7	10.8	5.2	9.6	8.3
O	Nafion®	S=O	534.5–535.5	2.5	2.3	2.9	2.4	2.0	2.6
F	Nafion®	C–F_2	688.9	37.9	30.4	23.7	31.4	25.5	27.8
F	Nafion®	C–OF_2, C–F_3	691.6	2.6	4.1	4.5	3.1	5.7	3.9

Table 3
Surface concentrations of carbon catalyst-support, ionomer and catalyst; detailed Nafion® compositions and featured weight ratios of the cathode catalyst layers analyzed by XPS. A relative accuracy of 1% for C, F and O is expected.

Element	Theoretical	Fresh	After 350 h	After 550 h		After 630 h (CO)	
			Inlet	Inlet	Outlet	Inlet	Outlet
	Surface composition (at.%)						
C-support	–	32.8	37.9	46.3	41.8	43.7	43.5
Pt catalyst	–	0.5	0.3	0.2	0.5	0.2	0.3
Nafion®	–	66.7	61.8	53.5	57.7	56.1	56.2
	Nafion® composition (at.%)						
F	60.0	60.8	60.0	57.4	61.8	60.7	60.2
C	30.8	31.3	30.9	30.3	28.8	30.8	28.9
O	7.7	6.7	7.2	10.7	7.7	7.0	8.9
S	1.5	1.2	1.9	1.6	1.6	1.6	2.1
	Weight ratios						
Pt catalyst/Pt–C	20.0	19.9	12.1	7.1	16.7	7.5	10.7
Nafion®/C-support	2.8	2.3	2.0	1.5	1.6	1.7	1.6

3.2.2. General XPS-based analysis (inlet zones)

The survey spectra of the two samples from the inlet zone of the CL aged under pure hydrogen and air for 350 h and 550 h are reported in Fig. 2(b) and (c). A silicon contamination of about 2–3 at.% arising from the gaskets is noticeable [13].

Regarding the atomic concentration changes of the CL from the inlet zone of the 550 h sample in Table 1, the surface concentrations of fluorine and platinum decrease from 40.5% to 28.1% and from 0.5% to 0.2% respectively, while the carbon and oxygen contents increase from 53.7% to 57.2% and from 4.5% to 13.7%, respectively.

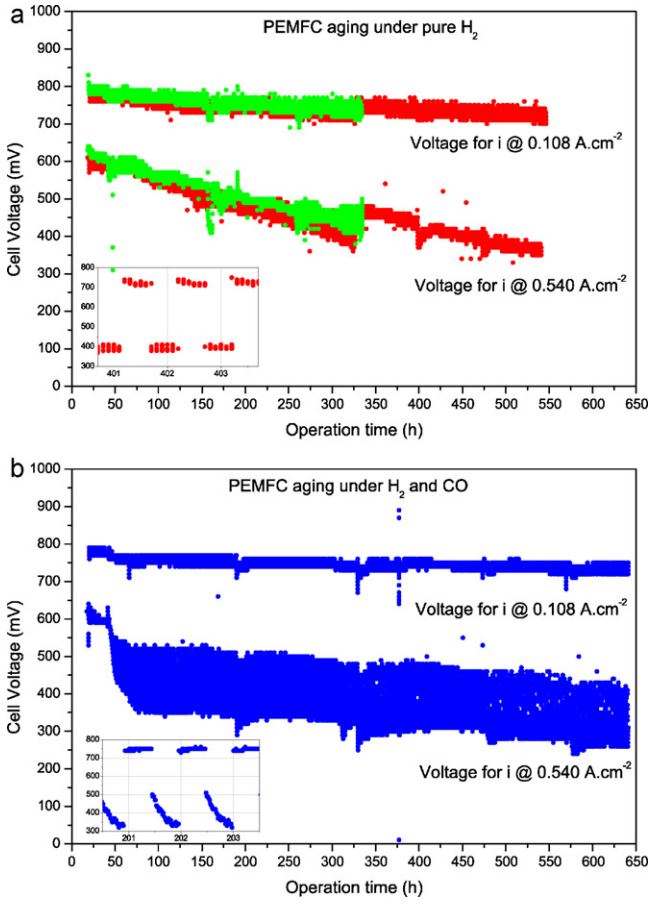

Fig. 7. Cell voltage evolutions under current cycling conditions (a) under pure H_2 for two experiment durations (in green 350 h, in red 550 h) (b) under H_2 and CO for 650 h. The first 22 h were performed under pure hydrogen and air, before introducing CO. The insets detail cell voltage evolutions over 3 h. (For interpretation of the references to color in this figure legend, the reader is referred to the web version of the article.)

The fitted high resolution spectra of carbon, oxygen, fluorine and platinum are displayed in Figs. 3(b) and (c), 4(b), 5(b) and 6(b). Although similar chemical states for carbon and oxygen are observed before and after fuel cell use, their relative proportions are different.

As seen in Figs. 3(b) and (c) and 4(b) there is a clear increase of the oxidized forms of carbon and of the high binding energy oxygen atoms. For example, the concentration of the oxidized forms of carbon for the inlet zone of the 550 h sample is increased by a factor two (Table 2). A part of the high binding energy oxygen atoms arises from the silicone gaskets contamination [38]. Up to 4–6 at.% of these atoms are bonded to Si to form Si–O bonds. It can be expected that an another part these additional oxygen atoms is bonded to carbon and form C–O bonds on the carbon catalyst-support surface. Thermodynamically, carbon catalyst-support can be electrochemically oxidized to CO_2 at quite low potentials. An intermediate CO_{surf} starts to form irreversibly on the carbon particle surface then is oxidized, this phenomenon being faster close to Pt nanoparticles [15,19,20]. The increase of C–O species on the C1s photoelectron line can be linked with carbon oxidation.

As seen in Figs. 3(b) and 5(b), there is also a decrease in the surface concentration of the ionomeric forms of carbon relative to the graphitic forms of carbon. Regarding, for example, the inlet zone of the 550 h sample in Tables 2 and 3, the concentration of fluorine and fluorinated carbon decrease jointly from 40.5% to 28.1% and from 20.9% to 14.8%, respectively. The ratio of concentrations is still close to the theoretical value of 2 fluorine for 1 fluorinated carbon. However, the O1s signal at the high binding energy (S–O bonds) remains nearly constant as well as the sulfur concentration.

In order to investigate quantitatively the possible ionomer degradation, the oxidation of the carbon catalyst-support and the loss of platinum, atomic percentage of each cathode CL components were calculated from experimental values from Table 2. A constant ratio between oxygen in acid sulfonic groups and oxygen in ether groups in the ionomer was assumed. The concentration of the additional oxygen atoms bonded to Si atoms or carbon groups was not taken into account. Results are summarized in Table 3. Regarding, for example, the inlet zone of the 550 h sample, the concentration of atoms related to the ionomer decreases from 66.7% to 53.5% indicating a loss of ionomer after aging.

Fig. 9(b) and (c) displays the atomic concentration of the carbon (graphitic and oxidized) in the carbon catalyst-support and the atomic concentration of the catalyst (metallic and oxidized) of the CL from the inlet zone in function of fuel cell operation time (data from Tables 2 and 3). The total amount of platinum is reduced with operation time but the metallic/oxidized ratio of catalyst is roughly constant. In the cathode catalyst layer, where high

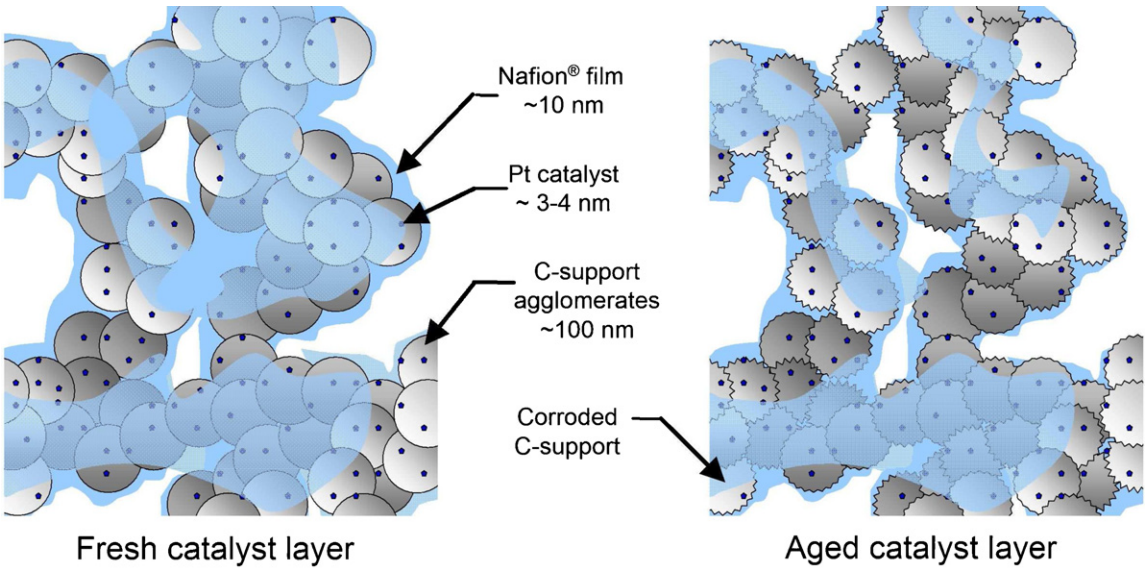

Fig. 8. Schematic view illustrating the aging of the cathode active layer under our experimental conditions. Carbon corrosion may cause the crumbling of the carbon catalyst-support and an increase of its roughness together with the loss of platinum. The ionomer is also probably degraded. The inelastic mean free path of photoelectrons in XPS is a few nanometer lengh, smaller than the caracteristic dimension of active layer components. As a consequence, the carbon concentration measured by XPS increase seemingly.

potentials are encountered, the platinum particules can dissolve, diffuse and recrystallise onto larger particles [20]. The resulting metallic/oxidized ratio from XPS would be lower since the inelastic mean free path of the photoelectrons is in the order of the caracteristic dimension of the catalyst particules. Thus, a nearly constant metallic/oxidized ratio may indicate weak modifications of the catalyst particle or may also be related to an electrochemical Oswald ripening process.

The degradation of the carbon catalyst-support leads to a slight evolution of the microstructure. A possible configuration consistent with our XPS results is shown in Fig. 8. This scheme illustrates the aging of the cathode active layer under our experimental conditions. Carbon oxidation may cause the crumbling of the carbon catalyst-support and an increase of its roughness together with a loss of platinum. The ionomer is also probably degraded. The inelastic mean free path of photoelectrons in XPS is a few nanometer lengh, smaller than the caracteristic dimension of active layer components. As a consequence, the carbon concentration measured by XPS increases seemingly.

3.2.3. Detailed XPS-based analysis: inlet vs. outlet zones

The atomic concentrations of the oxygen-rich (inlet) and oxygen-poor (outlet) zones of the cathodic CL samples aged under pure hydrogen and air for 550 h are reported in Table 1. The measured binding energies and the related chemical bondings of each component are reported in Table 2. CL components surface concentrations derived from XPS are presented in Table 3. For the outlet zone the surface concentration of fluorine decreased from 40.5% to 34.5%, while the carbon and oxygen content increased from 53.7% to 56.5% and from 4.5% to 7.6% respectively. The platinum concentration is almost unchanged. Aging of the oxygen-poor zone of the MEA follows the general trend described above for the oxygen rich zone: decrease of the Nafion® ionomer surface concentration relative to the carbon catalyst-support surface concentration. However, concerning the loss of platinum and the oxidation of carbon catalyst-support, aging is less dramatic. This is consistent with the fact having more cathode degradation in front of H_2-poor zones in agreement with our previous modeling results [15].

3.3. PEMFC aging under H_2 with CO

3.3.1. Performance degradation

Fig. 7(b) shows the cell voltage evolution with time under H_2 with 5 ppm CO. After introducing CO in hydrogen, a strong decrease of the voltage is observed followed by a lower mean degradation rate compared to that observed under pure H_2. The short-time scale potential decrease, in detailed view in Fig. 7(b), is explained through the gradual anodic potential increase as a consequence of the CO adsorption kinetics. This kind of behavior overlaps the long-time scale potential degradation [1].

3.3.2. General XPS-based analysis (inlet zones)

The survey spectrum of the sample aged under H_2 with 5 ppm CO and air for 630 h is displayed in Fig. 2(d). The silicon contamination arising from the gaskets is still noticeable. The fitted high resolution spectrum of carbon is displayed in Fig. 3(d), elemental composition changes are in Table 1 and the results of XPS decomposition are presented in Table 2. CL components surface concentrations are presented in Table 3 and Fig. 9.

Although similar carbon, fluorine, oxygen and platinum chemical states are observed before and after aging under H_2 + CO and air, their relative proportions are different. These significant changes in the elemental concentration are similar to those occurring in samples aged under pure hydrogen and air. The surface concentration of fluorine and platinum decreases and the carbon and oxygen content increases, which we previously attributed to a decrease of the Nafion® ionomer surface concentration compared to the surface concentration of the carbon catalyst-support.

From Fig. 9(a) and (b) there is an increase of the Nafion® ionomer surface concentration and a lower concentration of CO_{surf} species compared to the expected behavior under pure H_2 anode operation. Moreover, a higher catalyst concentration is observed (leading to a higher Pt-catalyst/Pt–C ratio in Table 3) compared to the expected behavior under pure H_2 anode operation. These results show that the cathode carbon catalyst-support corrosion is lower and mean less microstructural changes of the CL when CO is introduced in the anode side.

The anodic reactivity between the CO and the membrane crossover O_2, the last one being the “driving force” of the cath-

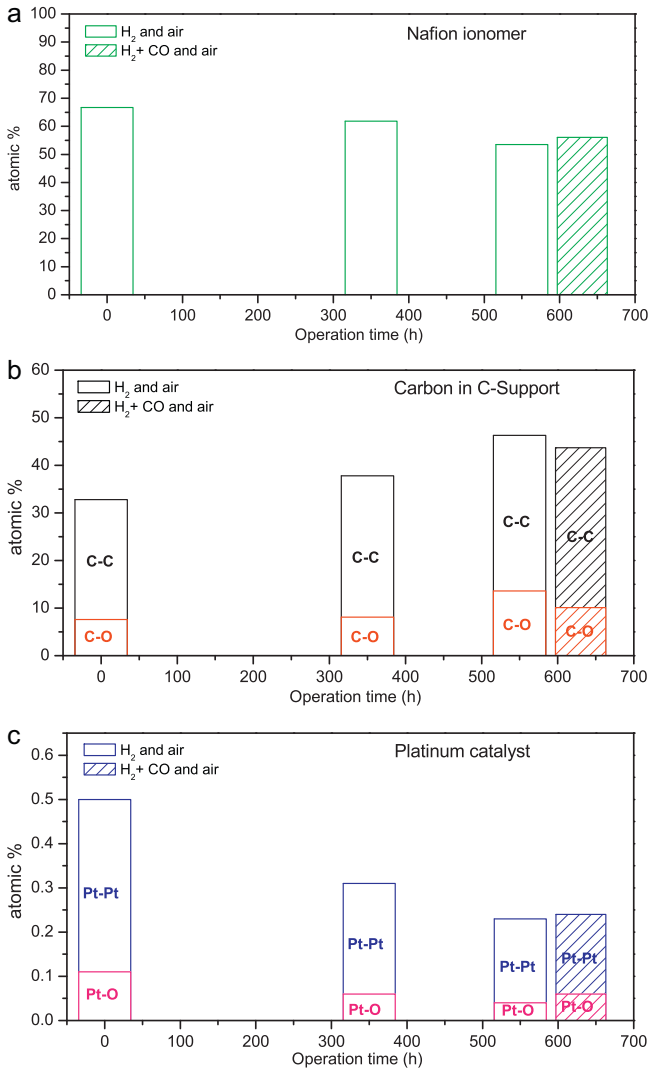

Fig. 9. Evolution in function of fuel cell operation time of the atomic concentrations of (a) Nafion® ionomer, (b) carbon in carbon catalyst-support (graphitic and oxidized) and (c) platinum catalyst (metallic and oxidized) from the inlet zone of the cathode catalyst layer as measured by XPS. A relative accuracy of 1% is expected for both the ionomer and the carbon catalyst-support.

ode to the anode proton pumping effect has been proposed to be the mechanism responsible for the cathode carbon catalyst-support corrosion mitigation [1]. CO reacts with O_2 on the surface of Pt, allowing the decrease of the anodic ORR rate and thus the reverse proton current and the cathode carbon corrosion. HOR and ORR are competing reactions occurring simultaneously on the anodic Pt surface, even under not completely fuel-starvated conditions. The ratio between the "surface seen by H_2" and the "surface seen by O_2" change with the operation current, this being related to the O_2 PEM permeation phenomena from the cathode to the anode. This surface ratio globally decreases as the current increases if the anodic H_2 stoechiometry is not sufficiently high (as in the experiments reported in this paper). CO injection introduces three more competing reactions on the same Pt surface: CO adsorption, CO electro-oxidation with water and O_2 reduction from CO, the last one being the responsible of getting reduced cathode C damage. This reaction between CO and pre-adsorbed O_2 on Pt is in fact very fast in PEMFC operating conditions in contrast to the one between O_2 and pre-adsorbed CO on Pt (air bleeding conditions), as recently demonstrated by ex situ experiments [42].

3.3.3. *Detailed XPS-based analysis: inlet vs. outlet*

The atomic concentrations of the oxygen rich (inlet) and oxygen poor (outlet) zones of the CL aged under hydrogen and CO and air for 630 h are reported in Table 1. The measured binding energies and the related chemical bondings of each component are reported in Table 2. CL component surface concentrations derived from XPS are presented in Table 3. In contrast to aging under pure hydrogen, the surface concentrations of the inlet and outlet zones are very similar. This result means that cathode aging is levelled under our experimental conditions.

4. Conclusions

XPS is used to successfully characterize the quantitative evolution of the chemical composition of the cathode CL materials (inlet and outlet zones) aged under fuel cell operation with pure hydrogen and air, and with 5 ppm CO contaminated hydrogen. In order to obtain accurate relative quantitative analysis all photoelectron lines were fitted in exactly the same way.

Aging under our experimental conditions induces a slight evolution of the microstructure as the carbon concentration measured by XPS increases seemingly. The concentration of CO_{surf} groups on the carbon catalyst-support increases, the platinum concentration decreases and the ionomer is probably degraded.

With pure hydrogen and air, the inlet zone is the most degraded. Aging of the oultlet zone is marked by a less dramatic oxidation of the carbon catalyst-support compared to the inlet zone.

When 5 ppm CO is introduced in the anode side cathode carbon catalyst-support corrosion is lower which means less microstructural changes of the CL. These results are in agreement with experimental-modeling work demonstrating that anodic CO contamination decreases the proton pumping effect and enhance the PEMFC durability [1,43]. The surface concentrations of the inlet and oultlet zones are very similar showing a homogeneous cathode aging.

XPS is a promising characterisation tool allowing a chemical description of the MEA CL. In a following paper, this technique will be used to compare the degradation of the inlet and outlet zones of anode and cathode CL under the above described experimental conditions.

Acknowledgments

This work was funded by the French Research Agency (ANR) through the program PAN-H and within the context of the POLIMPAC project.

References

[1] A.A. Franco, M. Guinard, B. Barthe, O. Lemaire, Electrochim. Acta 54 (2009) 5267.
[2] J.-H. Wee, Renew. Sustain. Energy Rev. 11 (2007) 1720.
[3] V. Lightner, Fuel Cell Stack Durability, Department of Energy Hydrogen Program Record, 2006.
[4] N. Garland, J. Marcinkoski, Fuel Cell System Cost, Department of Energy Hydrogen Program Record, 2008.
[5] W. Schmittinger, A. Vahidi, J. Power Sources 180 (2008) 1.
[6] S.D. Knights, K.M. Colbow, J. St-Pierre, D.P. Wilkinson, J. Power Sources 127 (2004) 127.
[7] Y. Shao, G. Yin, Y. Gao, J. Power Sources 171 (2007) 558.
[8] P.J. Ferreira, G.J. la O', Y. Shao-Horn, D. Morgan, R. Makharia, S. Kocha, H.A. Gasteiger, J. Electrochem. Soc. 152 (2005) A2256.
[9] A. Collier, H. Wang, X. Zi Yuan, J. Zhang, D.P. Wilkinson, Int. J. Hydrogen Energy 31 (2006) 1838.
[10] D.P. Wilkinson, J. St-Pierre, Durability, in: W. Wielstich, H.A. Gasteiger, A. Lamm (Eds.), Handbook of Fuel Cells – Fundamentals, Technology, Applications, John Wiley & Sons, Ltd., 2003 (Chapter 47).
[11] X. Cheng, Z. Shi, N. Glass, L. Zhang, J. Zhang, D. Song, Z.-S. Liu, H. Wang, J. Shen, J. Power Sources 165 (2007) 739.
[12] A.A. Franco, R. Coulon, R.F. de Morais, S.-K. Cheah, A. Kachmar, M.A. Gabriel, ECS Trans. 25 (2009) 65.

[13] M. Schulze, T. Knori, A. Schneider, E. Gülzow, J. Power Sources 127 (2004) 222.
[14] A.A. Franco, S. Passot, P. Fugier, C. Anglade, E. Billy, L. Guétaz, N. Guillet, E. De Vito, S. Mailley, J. Electrochem. Soc. 156 (2009) B410.
[15] A.A. Franco, M. Gerard, J. Electrochem. Soc. 155 (2008) B367.
[16] A.A. Franco, M. Tembely, J. Electrochem. Soc. 154 (2007) B712.
[17] A.A. Franco, P. Schott, C. Jallut, B. Maschke, Fuel Cells 7 (2007) 99.
[18] C.A. Reiser, L. Bregoli, T.W. Patterson, J.S. Yi, J. Deliang Yang, M.L. Perry, T.D. Jarvi, Electrochem. Solid-State Lett. 8 (2006) A273.
[19] F.A. de Bruijn, V.A.T. Dam, G.J.M. Janssen, Fuel Cells 08 (1) (2008) 3.
[20] R. Borup, J. Meyers, B. Pivovar, Y.S. Kim, R. Mukundan, N. Garland, D. Myers, M. Wilson, F. Garzon, D. Wood, P. Zelenay, K. More, K. Stroh, T. Zawodzinski, J. Boncella, J.E. McGrath, M. Inaba, K. Miyatake, M. Hori, K. Ota, Z. Ogumi, S. Miyata, A. Nishikata, Z. Siroma, Y. Uchimoto, K. Yasuda, K.-I. Kimijima, N. Iwashita, Chem. Rev. 107 (2007) 3904.
[21] B. Avasarala, R. Moore, P. Haldar, Electrochim. Acta, in press.
[22] X. Yu, S. Ye, J. Power Sources 172 (2007) 145.
[23] Y. Fujii, S. Tsushima, K. Teranishi, K. Kawata, T. Nanjo, S. Hirai, ECS Trans. 3 (2006) 735.
[24] T.F. Fuller, G. Gray, ECS Trans. 1 (2006) 345.
[25] W.R. Baumgartner, E. Wallnöfer, T. Schaffer, J.O. Besenhard, V. Hacker, V. Peinecke, P. Prenninger, ECS Trans. 3 (2006) 811.
[26] S. Maass, F. Finsterwalder, G. Frank, R. Hartmann, J. Power Sources 176 (2008) 444.
[27] E. Guilminot, A. Corcella, M. Chatenet, F. Maillard, F. Charlot, G. Berthomé, C. Iojoiu, J.-Y. Sanchez, E. Rossinot, E. Claude, J. Electrochem. Soc. 154 (2007) B1106.
[28] D. Riassetto, C. Holtzinger, M. Messaoud, S. Briche, G. Berthomé, F. Roussel, L. Rapenne, M. Langlet, J. Photochem. Photobiol. A: Chem. 202 (2009) 214.
[29] M Houmard, D.C.L. Vasconcelos, W.L. Vasconcelos, G. Berthomé, J.-C. Joud, M. Langlet, Surf. Sci. 603 (2009) 2698.
[30] M. Houmard, D. Riassetto, F. Roussel, A. Bourgeois, G. Berthomé, J.-C. Joud, M. Langlet, Surf. Sci. 602 (2008) 3364.
[31] M. Houmard, D. Riassetto, F. Roussel, A. Bourgeois, G. Berthomé, J.-C. Joud, M. Langlet, Appl. Surf. Sci. 254 (2007) 1405.
[32] Z.-B. Wang, P.-J. Zuo, Y.-Y. Chu, Y.-Y. Shao, G.-P. Yin, Int. J. Hydrogen Energy 34 (2009) 4387.
[33] F.-Y. Zhang, S.G. Advani, A.K. Prasad, M.E. Boggs, S.P. Sullivan, T.P. Beebe Jr., Electrochim. Acta 54 (2009) 4025.
[34] J.M. Rheaume, B. Müller, M. Schulze, J. Power Sources 76 (1998) 60.
[35] C. Chen, G. Levitin, D.W. Hess, T.F. Fuller, J. Power Sources 169 (2007) 288.
[36] C. Huang, K. Seng Tan, J. Lin, K. Lee Tan, Chem. Phys. Lett. 371 (2003) 80.
[37] M. Schulze, M. Lorenz, N. Wagner, E. Gülzow, Fresenius J. Anal. Chem. 365 (1999) 106.
[38] N. Ikeo, Y. Iijima, N. Niimura, M. Sigematsu, T. Tazawa, S. Matsumoto, K. Kojima, Y. Nagasawa, Handbook of X-ray Photoelectron Spectroscopy, JEOL, 1991.
[39] E.A. Hoffmann, T. Körtvélyesi, E. Wilusz, L.S. Korugic-Karasz, F.E. Karasz, A.Fekete Zoltan, J. Mol. Struct.: THEOCHEM 725 (2005) 5.
[40] B. Loppinet, G. Gebel, Langmuir 14 (1998) 1977.
[41] D.L. Wood, J. Chlistunoff, J. Majewski, R.L. Borup, J. Am. Chem. Soc. 131 (2009) 18096.
[42] S.K. Cheah, P. Gélin, V. Bernardet, O. Lemaire, A.A. Franco, in preparation.
[43] A.A. Franco, PEMFC degradation modeling and analysis. in: C. Hartnig, C. Roth (Eds.), Polymer electrolyte membrane and direct methanol fuel cell technology (PEMFCs and DMFCs) – Volume 1: Fundamentals and performance, Woodhead, Cambridge, 2011, in press.